Combining Nanoconfinement in Ag Core/Porous Cu Shell Nanoparticles with Gas Diffusion Electrodes for Improved Electrocatalytic Carbon Dioxide Reduction

Author

Junqueira, João RC, O'Mara, Peter B, Wilde, Patrick, Dieckhöfer, Stefan, Benedetti, Tania M, Andronescu, Corina, Tilley, Richard D, Gooding, J Justin, Schuhmann, Wolfgang

Published

2021

Journal Title

ChemElectroChem

Version

Version of Record (VoR)

DOI

https://doi.org/10.1002/celc.202100906

Combining Nanoconfinement in Ag Core/Porous Cu Shell Nanoparticles with Gas Diffusion Electrodes for Improved Electrocatalytic Carbon Dioxide Reduction

João R. C. Junqueira,[a] Peter B. O'Mara,[b] Patrick Wilde,[a] Stefan Dieckhöfer,[a] Tania M. Benedetti,[b] Corina Andronescu,[c] Richard D. Tilley,[b, d] J. Justin Gooding,[b] and Wolfgang Schuhmann*[a]

Bimetallic silver-copper electrocatalysts are promising materials for electrochemical CO_2 reduction reaction (CO_2RR) to fuels and multi-carbon molecules. Here, we combine Ag core/porous Cu shell particles, which entrap reaction intermediates and thus facilitate the formation of C_{2+} products at low overpotentials, with gas diffusion electrodes (GDE). Mass transport plays a crucial role in the product selectivity in CO_2RR. Conventional H-cell configurations suffer from limited CO_2 diffusion to the reaction zone, thus decreasing the rate of the CO_2RR. In contrast, in the case of GDE-based cells, the CO_2RR takes place under enhanced mass transport conditions. Hence, investigation of the Ag core/porous Cu shell particles at the same potentials under different mass transport regimes reveals: (i) a variation of product distribution including C_3 products, and (ii) a significant change in the local OH^- activity under operation.

Introduction

Alongside the increase in the concentration of atmospheric CO_2, the interest in suitable materials for the CO_2 reduction reaction (CO_2RR) to valuable fuels and chemicals is growing significantly.[1] The CO_2RR is a complex reaction that occurs via multi proton-coupled electron transfer steps and many different intermediates under the formation of various products.[2,3,4] The selectivity of single metals for the CO_2RR have been previously investigated. Ag, for instance, shows an almost exclusive formation of CO, whereas Cu is the only single metal reported to produce multi-carbon molecules; however, with insufficient selectivity and unsatisfactory long-term stability.[4–6] In bimetallic AgCu catalysts, the combination of two different active sites improves the product distribution through enhanced selectivity towards C_{2+} products at comparatively low overpotentials.[4,7] The improved performance originates from a reaction cascade, in which at the first step Ag centres can efficiently reduce CO_2 to CO at a low overpotential,[8] followed by further reduction of CO intermediate on Cu sites to C_{2+} molecules at a lower applied potential and with higher selectivity if compared to Cu-only catalysts.[6,9] The desorption of a CO molecule from one active site and the transport and re-adsorption at another one is known as CO spill-over mechanism.[10,11] In this context, bimetallic AgCu nanoparticles are an interesting material, where the structure of the particles strongly influences the CO_2RR product distribution.[4,12,13,14–16] For example, AgCu nanodimer particles showed a faradaic efficiency (FE) for ethylene of up to ~38%.[14]

Most studies with AgCu bimetallic catalysts use conventional H-cell set-ups, in which the catalyst-modified electrode is completely immersed in a CO_2-saturated electrolyte.[5,9,10,12,14] Assessing the CO_2RR performance of catalysts with this cell design has, however, inherent limitations, which are primarily related to the long CO_2 diffusion pathways. Hence slow mass transport from the bulk of the electrolyte to active centres of the catalyst. Therefore, CO_2 is quickly depleted in the vicinity of the active catalytic centres, limiting its conversion, and preventing the assessment of the full capability of the catalyst material (Scheme 1d). Moreover, in this scenario, the rate of the parasitic hydrogen evolution reaction (HER) is promoted. In contrast, gas diffusion electrodes (GDEs) are known to enable a higher flux of the gaseous reactant to the catalyst through shorter diffusional pathlengths leading to higher CO_2 concentration in the reaction

[a] J. R. C. Junqueira, Dr. P. Wilde, S. Dieckhöfer, Prof. Dr. W. Schuhmann
Analytical Chemistry – Center for Electrochemical Sciences (CES)
Faculty of Chemistry and Biochemistry,
Ruhr-Universität Bochum
Universitätsstraße 150,
D-44780 Bochum, Germany
E-mail: Wolfgang.Schuhmann@ruhr-uni-bochum.de
[b] P. B. O'Mara, Dr. T. M. Benedetti, Prof. Dr. R. D. Tilley, Prof. Dr. J. J. Gooding
School of Chemistry and Australian Centre for NanoMedicine
University of New South Wales
Sydney 2052, Australia
[c] Prof. Dr. C. Andronescu
Chemical Technology III
Faculty of Chemistry and CENIDE,
Center for Nanointegration
University Duisburg Essen
Carl-Benz-Straße 199, D-47057 Duisburg, Germany
[d] Prof. Dr. R. D. Tilley
Electron Microscope Unit
Mark Wainwright Analytical Centre
University of New South Wales
Sydney 2052, Australia

Supporting information for this article is available on the WWW under https://doi.org/10.1002/celc.202100906

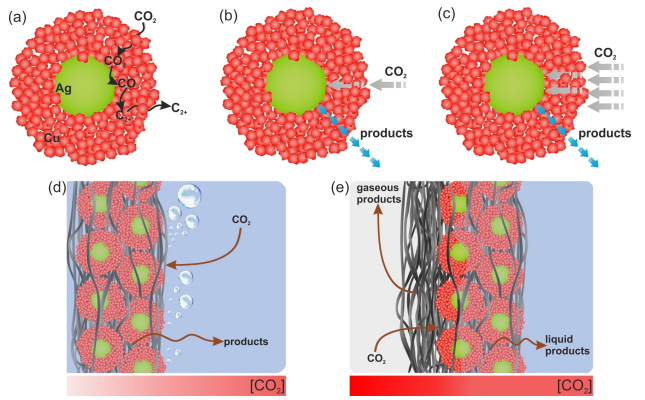

Scheme 1. (a) Representation of the cascade reaction in the Ag core/porous Cu shell particle. (b) The reaction is limited by CO_2 depletion from the bulk and only a small amount of CO_2 reaches the catalyst particle. (c) The reaction is limited by the CO_2 mass transport inside the porous Cu shell. (d) Comparison of the CO_2RR in an H-cell with the catalyst layer entirely immersed within the electrolyte and (e) the GDE-based electrochemical cell. Local CO_2 concentration is indicated by colour gradient with red colour indicating high and white indicating low concentrations.

zone (Scheme 1e) and establishing higher currents.[5,17,18] Cu–Ag tandem catalysts measured with a GDE show a production rate of around -160 mA/cm^2 for C_{2+} products.[19] The CuAg is not the only possible combination for cascade reactions, other tandem catalysts measured in GDE cells were reported with a high production rate for C_{2+} products reaching up to -367 mA/cm^2 with Cu/ZnO/C[20] and -415 mA/cm^2 using Cu/Ni–N–C.[21]

In contrast to bimetallic and tandem catalyst structures, where various active centres are directly exposed to the electrolyte, the Ag core/porous Cu shell catalyst used in this work exhibits a unique structure with a Ag core, which is surrounded by a porous Cu shell, such that the CO produced at the Ag core can react at the Cu shell without diffusion to the bulk (Scheme 1a).[22] Previously, we demonstrated that the porous channel system of these nanoparticles creates a nanoconfinement leading to a locally higher CO concentration within the Cu shell that ultimately results in the formation of more complex products such as *n*-propanol at a comparatively low overpotential.[15] The CO_2RR performance of these particles is sensitive to the applied potential. At more cathodic potentials the particles experience structural changes, in which the shell breaks apart with a concomitant loss of nanoconfinement.[16] Therefore, it is crucial to assess the selectivity of these particles under strict potential control.

The CO_2 to CO step is essential for the formation of C_{2+} products. Therefore, the Ag core/porous Cu shell particles activity can be limited by either (i) low CO_2 concentration at the reaction zone, caused by the H-cell constraints (Scheme 1b), or (ii) low CO_2 availability at the Ag core, caused by a restricted CO_2 transport within the Cu shell (Scheme 1c). We hence combined the Ag core/porous Cu shell particles with GDEs to eliminate the fundamental limitations of the H-cell configuration, allowing the direct comparison of the particles' selectivity under two CO_2 flux regimes. The measurements with the GDE cell allow for an evaluation of the catalyst's performance devoid of diffusional restraints and at higher currents. The presented results show an improvement in the CO_2RR activity and selectivity of the Ag core/porous Cu shell particles using a GDE as compared to a CO_2-saturated H-cell. Furthermore, only measurements in the GDE cell showed the formation of C_3 products, further emphasising the importance of the shorter CO_2 diffusion pathways. Measurements of the OH^- activity in close proximity of the operating electrodes reveal that there is a significant local variation of the OH^- activity for both H-cell and GDE cell. Nonetheless, the extent of these changes is more pronounced when the GDE cell is used.

Results and Discussion

Ag core/porous Cu shell particles were synthesised as described previously.[15,16] The particles exhibit a Ag core with ~46 nm diameter with a porous Cu shell with a thickness of ~25 nm (Figure 1 and Figure S1). The STEM images confirm the porosity of the Cu shells, which is a prerequisite for the transport of CO_2 to the silver core. To prevent inconsistencies related to subtle variations in particle size or catalyst structure, the same nanoparticle synthesis batch was used in all experiments. Electrodes were prepared by drop-casting a suspension of catalyst powder and PTFE particles in methanol onto carbon paper (Figure S2). New electrodes were used for each experiment performed at the different applied potentials or configurations of the electrochemical cell (Figure S3), and each electrode was measured only once to prevent influences from possible catalyst degradation.

The experiments with the GDE reached significantly higher currents than those performed in the H-cell (Figure 2, Figure S4 and Table S1). Due to the inherent existence of an uncompensated resistance (R_u) between the working and reference electrode, the actual potential at the working electrode differs from the nominal applied potential proportionally to the magnitude of the measured current. Therefore, all measurements were performed with an automatic iR_u compensation protocol (for further details, see SI and Figure S5). Three potentials of -0.50, -0.65 and -0.80 V *vs.* $RHE_{iRcor.}$ (all the potential values in this work are given in V *vs.* $RHE_{iRcor.}$, see supporting information) were selected for the measurement series to give catalytic currents of -0.7, -7.9 and -17.3 mA for the H-cell and -3.0, -18.6 and -106 mA for the GDE cell

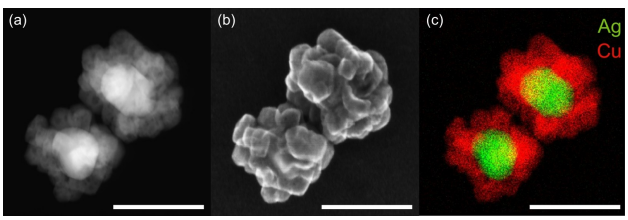

Figure 1. (a) STEM-DF, (b) SEM micrographs and (c) EDS colour map for Ag and Cu of the synthesised Ag core/porous Cu shell nanoparticles, scale bar corresponds to 100 nm.

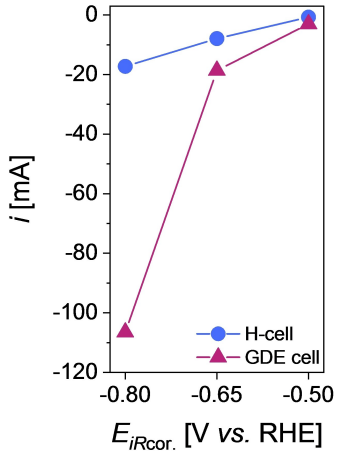

Figure 2. Average current *i* at the end of the 1-hour long chronoamperometry *vs.* E_{iRcor} at different applied potentials with the H-cell and GDE cell. Catalyst loading per electrode ~1.6 mg, n = 2.

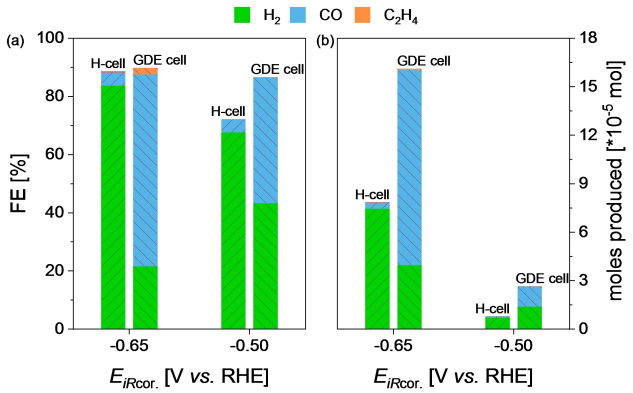

Figure 3. (a) Average faradaic efficiency and (b) mols of product formed for H_2, CO and C_2H_4 at −0.50 and −0.65 V *vs.* $RHE_{iRcor.}$ after 30 min with the H-cell and GDE cell. Catalyst loading per electrode ~1.6 mg, n = 2.

measurements. The measured currents were 4.2, 2.3 and 6.2 times higher at the three selected potentials when performed with the GDE cell. Such high current differences underscore the necessity of the automatic iR_u compensation since they would significantly influence the actual potential at the working electrode. Moreover, such differences in the measured currents between the two cell designs suggest that for the GDE cell there could be a significant variation of the pH value close to the reaction zone. These changes in the pH value would be a direct consequence of the consumption of H_2O and the release of OH^- during CO_2RR, as demonstrated in the half cell reactions for alkaline electrolytes (see supporting information).[2] Previously, the increase in the local pH value was shown to increase the production of C_2 products and suppress HER.[23,24]

To ensure comparable measurements, the CO_2RR experiments were performed in 1 M $KHCO_3$ as the electrolyte in both types of electrochemical cells (Figure S3). Gaseous products were separated and analysed using online gas chromatography, and liquid products were quantified with ^{1}H-NMR from interval aliquots (for experimental details, see supporting information). Apart from H_2, six major CO_2RR products, namely CO, ethylene (C_2H_4), formate (HCO_2H), acetate (CH_3CO_2H), ethanol (C_2H_5OH), and *n*-propanol (C_3H_7OH) were quantified. Methane (CH_4) and ethane (C_2H_6) were also identified, but with a faradaic efficiency of below 1%, and hence they were not considered further (Figure S6). The activity and selectivity of the CO_2RR in the GDE cell differed significantly from the results obtained in the H-cell. The effect of the cell design goes beyond merely increasing the maximum current. Rather, the range of products, and their distribution, changed substantially for the otherwise identical catalyst particles. At a working electrode potential of −0.50 V, CO and H_2 were mostly exclusively formed products with both cell designs. This potential was too low to invoke a significant formation of C_{2+} products on the Cu shell (Figure 3, Figure S6 and Table S2).

When measured in the H-cell, H_2 is by far the major product at all applied potentials with a faradaic efficiency ranging around 80% and it increases at larger bias potentials. The dominant HER leads to only a small partial current for the CO_2RR products. In contrast, the FE for H_2 is much smaller with the GDE cell ranging around 27% and it decreased at higher overpotentials. Moreover, when comparing the H-cell and GDE cell at the same potentials, the FE for H_2 decreased 4 times at −0.65 V from ~80% to ~20% and 5 times at −0.80 V from ~90% to ~16%. With the suppression of the HER, a larger portion of the current was used for the CO_2RR, consequently, using the GDE cell yielded superior FEs for all detected CO_2 reduction products at all measured potentials (Figure 3a and Figure S6). In general, with the faster CO_2 mass transport, the GDE presents a more favourable environment for the CO_2RR over the undesired HER. Whereas all CO_2RR products add up to a FE of around 8% in the case of the H-cell, this value increases to approximately 70% in the case of the GDE cell at −0.65 V. The FE of CO increases around 13 times, whereas the increase in the C_{2+} products is around 7 times at −0.65 V. As a consequence of higher faradaic efficiencies, the use of the GDE cell increased significantly the total formed moles of CO_2RR products (Figure 3b). At −0.65 V, the amount of H_2 produced was two times smaller for the GDE than for the H-cell, whereas the moles of CO and C_2H_4 increased 32 and 17 times, respectively. Furthermore, the partial current for ethylene increased by a factor of 16 at −0.65 V in the case of the GDE cell (Table S3). These results suggest that measurements in CO_2-saturated electrolytes with a conventional H-cell do not allow for a comprehensive assessment of the intrinsic properties of a catalyst material due to the rapid depletion of CO_2 favouring the HER.

The results show, that the proposed cascade mechanism inside the nanoconfined environment within the porous Cu shell is limited by the CO formation rate at the Ag core. It is revealed, that with the H-cell that the small CO production stems neither from a low intrinsic activity of the Ag cores nor a CO_2 diffusion barrier through the porous Cu shell, but rather from mass transport limitations inherent to the H-cell configuration and the low solubility of CO_2. Once the particles are placed on a GDE the limited CO_2 mass transport to the particles

is mitigated, and the activity of Ag core/porous Cu shell nanoparticles as a CO_2 reduction catalyst can be accurately addressed and assessed.

The beneficial effects of the GDE become even more apparent at more cathodic potentials, where the previously described trends between the two cell geometries are confirmed. At −0.80 V the FE for H_2 decreased around 5 times using the GDE cell, whereas the FE for CO increased by 12 times and by 10 times for C_{2+} products in comparison to the H-cell (Figure S6 and Table S2). These results highlight the selectivity for cascade products (Figure 4). Furthermore, the formation of cascade products increased by about 10 times at −0.80 V compared to −0.65 V with a FE of ~17% for ethylene and ~11% for ethanol in the case of the GDE cell. The FE and the sum of C_{2+} products partial current increased from 2.3% and −0.5 mA in an H-cell, to 29% and −51 mA with the GDE cell at −0.8 V. The amount of C_2H_4 increased by a factor of 62 when using the GDE cell from 7.8 x10^{-7} to 4.9 x10^{-5} mols (Figure 4b).

We reported previously that the structure of the bimetallic core/shell particles changes at this potential (for further details, see SI and Figures S7).[16] Based on the proposed cascade mechanism, the formation of multi-carbon products is promoted when the original particle structure is present allowing the nanoconfinement of CO. Therefore, the integrity of the Ag core/porous Cu shell particles needs to be confirmed which is possible by assessing changes in the product distribution over electrolysis time. If the ratio between the FE of C_{2+} and CO ($FE_{C2+/CO}$) exhibits a constant value, the particles are considered stable during the measurement.[16] However, if this value decreases over time, the porous Cu shell is disintegrating and the nanoconfinement capability necessary for the C_{2+} product formation is lost. Figures S9a and b show that the FE for CO and C_{2+} remained similar throughout the whole experiment at −0.50 and −0.65 V for both H-cell and GDE cell experiments. More importantly, the $FE_{C2+/CO}$ ratio was relatively constant with a slight decrease at −0.65 V, revealing the integrity of the Ag core/porous Cu shell particles during the measurement. In contrast, at −0.80 V (Figure S9c) a significant increase of the FE for CO in combination with a decrease in the FE for C_{2+} is observed with a decrease of the $FE_{C2+/CO}$ ratio by more than 5 times during the measurement, which indicates the loss of the porous Cu shell. These observations are valid for both H-cell and GDE cell, allowing the conclusion that the structural changes of the particles take place in a similar manner regardless of the used electrochemical cell configuration. The particles are stable at −0.50 and −0.65 V but lose their structure at −0.80 V.

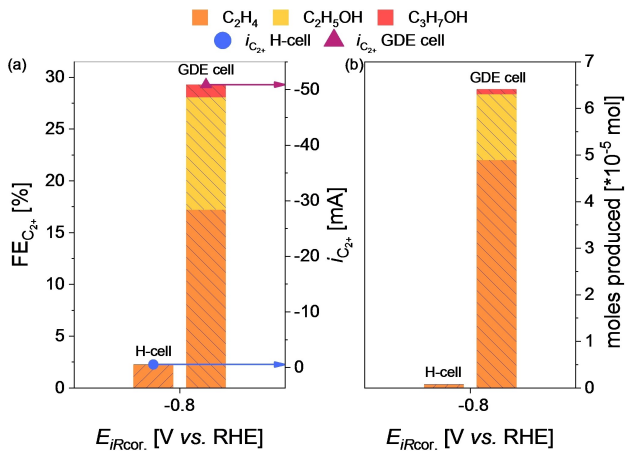

Figure 4. (a) Average FE (left Y-axis) of cascade products (C_{2+} = C_2H_4 + C_2H_5OH + C_3H_7OH) and the sum of C_{2+} products partial current (right Y-axis) and (b) number of moles produced at −0.80 V *vs.* $RHE_{iRcor.}$ after 30 min with the H-cell and GDE cell. Catalyst loading per electrode ~1.6 mg, n = 2.

However, the measurements at −0.80 V in a GDE cell still allow us to assess the performance of the bimetallic catalyst under increased CO_2 mass transport conditions enabling the assessment of the whole activity potential of the catalytic material for the CO_2RR. Another indication that the use of a GDE cell at −0.80 V is beneficial for the investigation of CO_2RR catalysts is that at this potential a significant increase in the amount of C_3 products was shown, with a FE for *n*-propanol reaching up to 1%. Furthermore, one additional C_3 product, namely allyl alcohol, was detected in the GDE cell. Allyl alcohol was not formed in the H-cell measurements nor our earlier studies[15,16] with such particles (Figure S8).

During CO_2RR in alkaline electrolytes H_2O is continuously consumed of and OH^- is generated, leading to an accumulation of OH^- ions in close proximity to the reaction zone dependent on the reaction rate. Such a change in the local pH value may affect the product distribution of the electrocatalytic process.[23,24] To investigate these changes a positioned Pt microelectrode was used as a probe to determine the variation of the local activity ratios of OH^- and H_2O during CO_2RR with the H-cell and GDE cell configurations at different applied potentials (Figure S10). In these measurements, a Pt microelectrode was firstly positioned in close proximity to the electrode with shear-force based scanning electrochemical microscopy (SECM) (Figure S11).[25] The sensitivity for the local OH^-/H_2O activity ratios can be extracted from the PtO reduction peak potential ($E_{PtO\text{-}red.\ peak}$) *vs.* Ag|AgCl|3 M KCl reference electrode (data given in mV). In more alkaline electrolytes, the reduction of the PtO takes place at more cathodic potentials (see SI). The experiments were performed using a series of potential pulses. First, a potential equivalent to OCP was applied at the particle-modified electrode (−250 mV *vs.* Ag|AgCl|3 M KCl) followed by a cathodic potential, and to finish OCP was applied again. The particle modified electrode was switched between "ON" and "OFF", while measuring the local OH^-/H_2O activity ratio. Figure 5 shows the variation of the $E_{PtO\text{-}red.\ peak}$ measured at the Pt microelectrode when different potentials were applied at the Ag core/porous Cu shell modified electrode for both cell designs. A significant cathodic shift of the $E_{PtO\text{-}red.\ peak}$ was observed after applying the potential in both configurations, followed by an anodic shift when OCP was applied. The results indicate the local increase in the pH value when CO_2RR and the potentially competing HER are taking place. Furthermore, at higher applied potential, the $E_{PtO\text{-}red.\ peak}$ was as expected more negative. The $E_{PtO\text{-}red.\ peak}$ shifts were more pronounced in the GDE cell (Figure 5c) in comparison to the H-cell (Figure 5a). Hence, these experimental data show that a

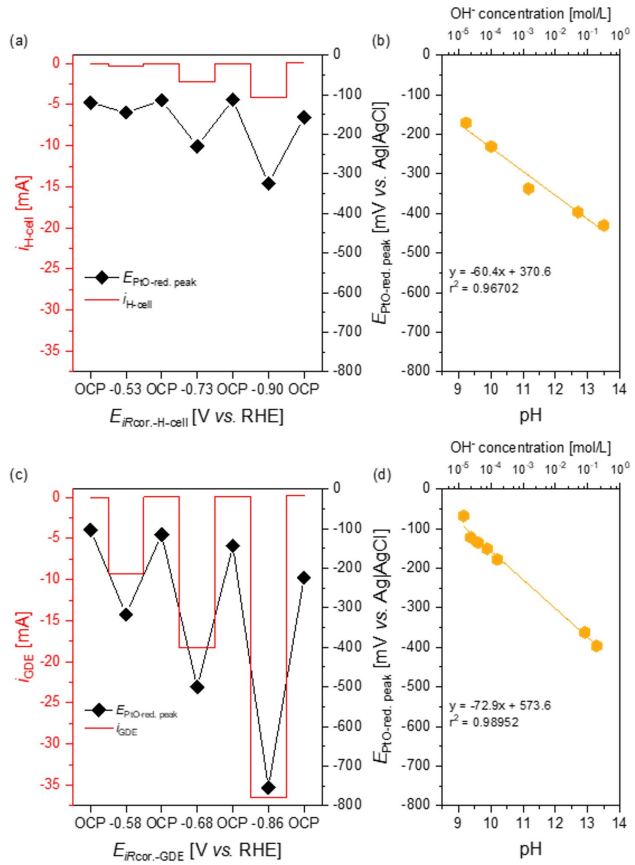

Figure 5. (a) Average current at the H-cell working electrode at different applied potentials (left Y-axis, line plot) and PtO reduction potential peak (right Y-axis, symbol and line plot) in CO_2-saturated 1 M $KHCO_3$. (b) Variation of the PtO reduction peak potential in solutions of different pH values. (c) Average current at the GDE cell working electrode at different applied potentials (left Y-axis, line plot) and PtO reduction potential peak (right Y-axis, symbol and line plot) in Ar-saturated 1 M $KHCO_3$ (d) variation of the PtO reduction potential peak in solutions of different pH values. Both working electrodes were prepared with ~1 mg/cm^2 of Ag core/porous Cu shell. $E_{PtO\text{-}red.\ peak}$ values extracted from the results in Figures S12 and S13.

more drastic local alkalinisation is obtained with a GDE than the H-cell.[18] The obtained values of $E_{PtO\text{-}red.\ peak}$ at different applied potentials can be compared with the measured values from the Pt probe calibration in solutions of different pH values (Figures 5b and d and Figure S13). Under operation at −0.68 and −0.86 V the GDE cell reached a local activity ratio of OH^-/H_2O higher than in 1 M KOH. These changes in the pH value support the effect on the product distributions. The results from the GDE cell showed a continuous decrease in the FE for H_2 at higher applied currents (Figure S6) and an increase in the CO_2RR. This can be explained by a combination of a shorter CO_2 diffusion pathlength provided by the gas diffusion layer and the high local OH^- activities obtained with this cell configuration.

Conclusion

In summary, the activity and selectivity of the Ag core/porous Cu shell nanoparticles are limited in an H-cell configuration, which precluded the comprehensive assessment of the full catalytic potential of this and presumably other nanostructured catalysts. In a GDE cell configuration, superior catalytic activity and selectivity for the CO_2RR were observed, resulting in larger currents and higher FE for CO_2RR products. The results elucidated that the particles were limited by the mass transport of reactants to the catalyst, and not within the porous Cu shell. To compare the results obtained with different reactors, it was vital to perform the measurements with automatic *iR* compensation to assure that the actual potential at the working electrode was independent of the measured current. Hence, the product distribution could be compared at the same applied potential using different cell designs. When the CO_2 mass transport limitations were removed using the GDE cell, a significant decrease in H_2 formation followed by an increase in CO_2RR products formation was observed. The results reveal that the CO_2RR performance of the Ag core/porous Cu shell particles improved at increased CO_2 mass transport conditions and higher currents. A significant increase in the FE for C_2 and C_3 products were observed when the catalyst particles were measured in the GDE cell. The measurement results highlight the distinct difference in the electrochemical environment in terms of the local pH value between H-cell and GDE cell, with alkalinisation being more pronounced in the case of the GDE cell. Hence, the GDE cell configuration grants improved conditions to evaluate the performance of the electrocatalyst material for the CO_2RR concomitantly making HER less favourable.

Acknowledgements

This project has received funding from the European Research Council (ERC) under the European Union's Horizon 2020 research and innovation programme (grant agreement CasCat [833408]) as well as from the Deutsche Forschungsgemeinschaft (DFG, German Research Foundation) in the framework of the research unit FOR 2397e2 (276655237). C.A. acknowledges funding by the BMBF in the framework of the NanomatFutur project "MatGasDif" (03XP0263). The Australian team acknowledges funding from the Australian Research Council (DP190102659, RDT, WS and DP210102698, JJG). Open Access funding enabled and organized by Projekt DEAL.

Conflict of Interest

The authors declare no conflict of interest.

Keywords: AgCu nanoparticles · CO_2 reduction · C_{2+} products · gas diffusion electrode · local pH

[1] R. K. Pachauri, L. Meyer, *Climate change 2014. Synthesis report*, Intergovernmental Panel on Climate Change, Geneva, Switzerland, **201**
[2] Z. Sun, T. Ma, H. Tao, Q. Fan, B. Han, *Chem* **2017**, *3*, 560.

[3] a) B. Khezri, A. C. Fisher, M. Pumera, *J. Mater. Chem. A* **2017**, *5*, 8230; b) L. Fan, C. Xia, F. Yang, J. Wang, H. Wang, Y. Lu, *Sci. Adv.* **2020**, *6*, eaay3111.
[4] G. Wang, J. Chen, Y. Ding, P. Cai, L. Yi, Y. Li, C. Tu, Y. Hou, Z. Wen, L. Dai, *Chem. Soc. Rev.* **2021**, *50*, 4993.
[5] K. Jiang, Y. Huang, G. Zeng, F. M. Toma, W. A. Goddard, A. T. Bell, *ACS Energy Lett.* **2020**, *5*, 1206.
[6] Y. Hori in *Handbook of Fuel Cells* (Eds.: W. Vielstich, A. Lamm, H. A. Gasteiger, H. Yokokawa), John Wiley & Sons, Ltd, Chichester, UK, **2010**.
[7] a) C. W. Li, J. Ciston, M. W. Kanan, *Nature* **2014**, *508*, 504; b) W. Zhu, B. M. Tackett, J. G. Chen, F. Jiao in *Topics in Current Chemistry Collections* (Ed.: M. Shao), Springer International Publishing, Cham, **2020**, pp. 105–125; c) A. Vasileff, C. Xu, Y. Jiao, Y. Zheng, S.-Z. Qiao, *Chem* **2018**, *4*, 1809; d) C. G. Morales-Guio, E. R. Cave, S. A. Nitopi, J. T. Feaster, L. Wang, K. P. Kuhl, A. Jackson, N. C. Johnson, D. N. Abram, T. Hatsukade, C. Hahn, T. F. Jaramillo, *Nat. Catal.* **2018**, *1*, 764.
[8] Y. Hori, K. Kikuchi, S. Suzuki, *Chem. Lett.* **1985**, *14*, 1695.
[9] C. W. Li, M. W. Kanan, *J. Am. Chem. Soc.* **2012**, *134*, 7231.
[10] D. Ren, B. S.-H. Ang, B. S. Yeo, *ACS Catal.* **2016**, *6*, 8239.
[11] J. Gao, H. Zhang, X. Guo, J. Luo, S. M. Zakeeruddin, D. Ren, M. Grätzel, *J. Am. Chem. Soc.* **2019**, *141*, 18704.
[12] S. Lee, G. Park, J. Lee, *ACS Catal.* **2017**, *7*, 8594.
[13] a) T. T. H. Hoang, S. Verma, S. Ma, T. T. Fister, J. Timoshenko, A. I. Frenkel, P. J. A. Kenis, A. A. Gewirth, *J. Am. Chem. Soc.* **2018**, *140*, 5791; b) A. Herzog, A. Bergmann, H. S. Jeon, J. Timoshenko, S. Kühl, C. Rettenmaier, M. Lopez Luna, F. T. Haase, B. Roldan Cuenya, *Angew. Chem. Int. Ed.* **2021**, *60*, 7426; c) D. Higgins, A. T. Landers, Y. Ji, S. Nitopi, C. G. Morales-Guio, L. Wang, K. Chan, C. Hahn, T. F. Jaramillo, *ACS Energy Lett.* **2018**, *3*, 2947; d) D. Ren, J. Gao, S. M. Zakeeruddin, M. Grätzel, *Chimia* **2019**, *73*, 928.
[14] J. Huang, M. Mensi, E. Oveisi, V. Mantella, R. Buonsanti, *J. Am. Chem. Soc.* **2019**, *141*, 2490.
[15] P. B. O'Mara, P. Wilde, T. M. Benedetti, C. Andronescu, S. Cheong, J. J. Gooding, R. D. Tilley, W. Schuhmann, *J. Am. Chem. Soc.* **2019**, *141*, 14093.
[16] P. Wilde, P. B. O'Mara, J. R. C. Junqueira, T. Tarnev, T. M. Benedetti, C. Andronescu, Y.-T. Chen, R. D. Tilley, W. Schuhmann, J. J. Gooding, *Chem. Sci.* **2021**, *12*, 4028.
[17] a) M. Duarte, B. de Mot, J. Hereijgers, T. Breugelmans, *ChemElectroChem* **2019**, *6*, 5596; b) L.-C. Weng, A. T. Bell, A. Z. Weber, *Phys. Chem. Chem. Phys.* **2018**, *20*, 16973; c) N. T. Nesbitt, T. Burdyny, H. Simonson, D. Salvatore, D. Bohra, R. Kas, W. A. Smith, *ACS Catal.* **2020**, *10*, 14093.
[18] T. Burdyny, W. A. Smith, *Energy Environ. Sci.* **2019**, *12*, 1442.
[19] C. Chen, Y. Li, S. Yu, S. Louisia, J. Jin, M. Li, M. B. Ross, P. Yang, *Joule* **2020**, *4*, 1688.
[20] Z. Li, R. M. Yadav, L. Sun, T. Zhang, J. Zhang, P. M. Ajayan, J. Wu, *Appl. Catal. A* **2020**, *606*, 117829.
[21] X. She, T. Zhang, Z. Li, H. Li, H. Xu, J. Wu, *Cell. Rep. Phys. Sci.* **2020**, *1*, 100051.
[22] J. Wu, X. Wang, Q. Wang, Z. Lou, S. Li, Y. Zhu, L. Qin, H. Wei, *Chem. Soc. Rev.* **2019**, *48*, 1004.
[23] K. J. P. Schouten, E. Pérez Gallent, M. T. Koper, *J. Electroanal. Chem.* **2014**, *716*, 53.
[24] R. Kortlever, J. Shen, K. J. P. Schouten, F. Calle-Vallejo, M. T. M. Koper, *J. Phys. Chem. Lett.* **2015**, *6*, 4073.
[25] a) A. Botz, J. Clausmeyer, D. Öhl, T. Tarnev, D. Franzen, T. Turek, W. Schuhmann, *Angew. Chem. Int. Ed.* **2018**, *57*, 12285; b) S. Dieckhöfer, D. Öhl, J. R. C. Junqueira, T. Quast, T. Turek, W. Schuhmann, *Chem. Eur. J.* **2021**, *27*, 5906; c) N. Sikdar, J. R. C. Junqueira, S. Dieckhöfer, T. Quast, M. Braun, Y. Song, H. B. Aiyappa, S. Seisel, J. Weidner, D. Öhl, C. Andronescu, W. Schuhmann, *Angew. Chem. Int. Ed.* **2021**, *60*, 23427.

Manuscript received: July 3, 2021
Revised manuscript received: November 18, 2021
Accepted manuscript online: November 24, 2021